RadioGraphics

Cardiac MR Imaging Assessment Following Tetralogy of Fallot Repair[1]

Karen I. Norton, MD • Carrie Tong, MD • Ronald B. J. Glass, MD
James C. Nielsen, MD

ONLINE-ONLY CME

See www.rsna.org/education/rg_cme.html.

LEARNING OBJECTIVES

After reading this article and taking the test, the reader will be able to:

- List the anatomic features of tetralogy of Fallot and some common sequelae.
- Describe the surgical procedures used to repair tetralogy of Fallot.
- Discuss the technical aspects of cardiac MR imaging and the benefits of using this modality in patients who undergo repair of tetralogy of Fallot.

TEACHING POINTS

See last page

Survivors of tetralogy of Fallot (TOF) repair constitute a large and growing population of patients. Although postsurgical outcome is generally favorable, as these patients move into adulthood, late morbidity is becoming more prevalent and the notion that TOF has been "definitively repaired" is increasingly being challenged. Recent evidence suggests that adverse long-term postsurgical outcome is related to chronic pulmonary regurgitation, right ventricular dilatation, and deteriorating ventricular function. Cardiac magnetic resonance (MR) imaging has been established as an accurate technique for quantifying ventricular size, ejection fraction, and valvular regurgitation. Cardiac MR imaging does not expose the patient to ionizing radiation and is therefore ideal for serial postsurgical follow-up. Familiarity with the anatomic basis of TOF, the surgical approaches to repair, and postrepair sequelae is essential for performing and interpreting cardiac MR imaging examinations. For example, awareness of the complications and sequelae that can occur will assist in determining when to intervene to preserve ventricular function and will improve long-term outcome. Technical facility is necessary to tailor the examination to the individual patient (eg, familiarity with non-breath-hold modifications that allow evaluation of young and less compliant patients). The radiologist can play an essential role in the treatment of patients with repaired TOF by providing noninvasive anatomic and physiologic cardiac MR imaging data. Further technologic advances in cardiac MR imaging are likely to bring about new applications, better normative data, and more examinations that are operator independent.

SUPPLEMENTAL MATERIAL

Movie clips to supplement this article are available online at radiographics.rsnajnls.org/cgi/content/full/26/1/197/DC1.

Abbreviations: FSE-DIR = fast spin-echo with double inversion recovery, LV = left ventricle, MIP = maximum intensity projection, PR = pulmonary regurgitation, RV = right ventricle, SSFP = steady state free precession, TOF = tetralogy of Fallot, 3D = three-dimensional, TR = tricuspid regurgitation, 2D = two-dimensional, VSD = ventricular septal defect

RadioGraphics 2006; 26:197–211 • **Published online** 10.1148/rg.261055064 • **Content Codes:** CA MR PD

[1]From the Departments of Radiology (K.I.N., C.T., R.B.J.G., J.C.N.) and Pediatric Cardiology (J.C.N.), Mount Sinai Hospital, Mount Sinai School of Medicine, 1 Gustave L. Levy Place, New York, NY 10029. Presented as an education exhibit at the 2004 RSNA Annual Meeting. Received March 17, 2005; revision requested April 27 and received June 1; accepted June 2. All authors have no financial relationships to disclose. **Address correspondence to** K.I.N. (e-mail: *sobelnort@aol.com*).

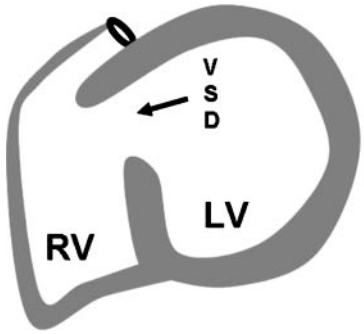

CONSISTENT FEATURES

•ANTERIOR MALALIGNMENT OF THE CONAL SEPTUM

•VSD

VARIABLE FEATURES

•INFUNDIBULAR NARROWING, PULMONIC STENOSIS, PULMONARY ARTERY ATRESIA

Figure 1. Drawing illustrates TOF. *LV* = left ventricle, *RV* = right ventricle, *VSD* = ventricular septal defect. Both the consistent features and the variable features of this pathologic condition are listed at right.

Introduction

Tetralogy of Fallot (TOF), the most common congenital heart defect associated with cyanosis and pulmonary undercirculation, accounts for approximately 6%–10% of all cases of congenital heart disease (1,2). Although the prognosis for patients who have undergone surgical repair is favorable (early mortality rate <2%), residual defects, complications, and sequelae are common (3–7). After undergoing repair, patients commonly have a variable degree of pulmonary regurgitation (PR). Over long-term follow-up, right ventricular (RV) dilatation and dysfunction, atrial and ventricular arrhythmias, congestive heart failure, and sudden death may occur. In a recent long-term follow-up study, the annualized risk of death increased substantially 25 years after surgical repair, with the mortality rate increasing from 0.24% to 0.94% (3). Restoring pulmonary valve function, and thereby reducing the substrate for RV dilatation, has been shown to decrease RV size and improve symptoms (8–15). The impact on RV systolic function, arrhythmia, and mortality rate has yet to be definitively demonstrated (9,11).

Teaching Point

The effectiveness of ultrasonography in providing comprehensive evaluation during long-term treatment of these patients is often limited due to the loss of adequate acoustic windows in older patients, coupled with the inability of echocardiography to help quantify RV size or function or the percentage of valvular regurgitation. Cardiac magnetic resonance (MR) imaging is a noninvasive method that allows serial follow-up of postsurgical patients without exposure to ionizing radiation or use of iodinated contrast material. Cardiac MR imaging can be used to quantify ventricular size, ejection fraction, and regurgitation. Adequate familiarity with the anatomic, clinical, and cardiac MR imaging appearances of TOF is important for optimizing the diagnostic yield of this imaging modality. Facility with the technical aspects of cardiac MR imaging is essential for producing high-quality images, especially in the potentially less compliant pediatric population. In this article, we review the anatomic features of TOF. In addition, we discuss cardiac MR imaging in terms of *(a)* advantages and disadvantages in TOF patients; *(b)* basic imaging techniques; and *(c)* assessment of ventricular mass, volume, and flow. We also discuss and illustrate common postsurgical complications of TOF repair.

Anatomic Features of TOF

The anatomic abnormality in TOF is failure of fusion of the conal and ventricular septa (Fig 1). This anterior malalignment of the conal septum leads to the classic tetrad of findings: subaortic VSD, an overriding aortic valve, RV infundibular stenosis, and subsequent RV hypertrophy (Fig 2). A right-sided aortic arch is seen in 25% of cases (2). Symptoms (cyanosis or congestive heart failure) are related to the degree of RV outflow tract obstruction (infundibular narrowing).

TOF with pulmonary valve atresia, also known as pulmonary atresia with VSD, is the most severe form of TOF, accounting for 2.5%–4% of all cases of congenital heart disease (Fig 3) (2). The degree of cyanosis varies with the number and size of systemic-to-pulmonary collateral vessels. The presence and size of the mediastinal pulmonary arteries dictates the surgical approach. When pulmonary arteries are adequate in size, an RV–pulmonary artery conduit is placed and the VSD

Figure 2. TOF in a 2-month-old boy. Frontal radiograph demonstrates a boot-shaped heart with an uplifted apex secondary to RV hypertrophy and a concave main pulmonary artery segment. The lungs appear to be undercirculated.

Figure 3. Pulmonary atresia with VSD in a 6-year-old boy. Frontal radiograph reveals extensive lacy, reticular pulmonary markings secondary to systemic-to-pulmonary collateral flow to the lungs. A right-sided aortic arch (arrow) is also seen.

is closed. If there are lung segments that are supplied by collateral vessels alone, attempts are made to incorporate these vessels into the repair procedure. Although gadolinium-enhanced MR angiography is becoming a critical adjunct to the presurgical evaluation of affected patients, defining course and lung supply (dual supply from collateral and native pulmonary arteries versus collateral vessels alone) is accomplished mainly with cardiac catheterization. Three-dimensional MR angiography can provide a "road map" to aid in catheterization planning and, eventually, in surgical repair (Fig 4) (16).

Figure 4. Uncorrected pulmonary atresia with VSD in a male infant. Coronal maximum-intensity-projection (MIP) image demonstrates a large aorta–pulmonary artery collateral vessel (arrow).

The preoperative assessment of infants with TOF is accomplished effectively with two-dimensional (2D) echocardiography alone in the vast majority of patients. Assessment is focused on exclusion of associated lesions, precise measurement of the pulmonary valve annulus and branch pulmonary arteries, and definition of the course of the proximal coronary arteries, since a coronary artery that crosses the surface of the RV outflow tract alters the surgical approach.

Cardiac MR Imaging

Advantages and Disadvantages in TOF Patients

Cardiac MR imaging has the advantage of being a noninvasive approach for the pre- and postoperative evaluation of patients with TOF, without the

Table 1
Technical Information for Cardiac MR Imaging

	Type of Imaging						
	FSE-DIR		SSFP				
Parameter	Breath-Hold	Free Breathing	Breath-Hold	Free Breathing	Cine PC	FSPGRE	3D MR Angiography
Flip angle (°)	90	90	40	40	20	15	30–45
Field of view (cm)	26–40	20–36	36–40	30–40	24–32	30–40	30–40
Matrix	256 × 192	192 × 192	224 × 192	160 × 128	256 × 128	512 × 192	256 × 160
Section thickness (mm)	3–6	3–6	7–8	5–7	5–6	5–9	1.2–3.0
VPS/ETL	24–32	24	14–18	10–16	2–4	· · ·	· · ·
Repetition time (msec)	· · ·	· · ·	· · ·	· · ·	· · ·	15	· · ·
Echo time (msec)	40	40	Minimum full	Minimum full	Minimum full	Minimum	Minimum full
rBW (kHz)	31.2	31.2	125	125	31.2	31.2	31.2
Signals acquired	1–2	3–4	1	3–4	3	1	0.5–1

ETL = echo train length, FSE-DIR = fast spin-echo with double inversion recovery, FSPGRE = fast spoiled gradient-recalled echo, rBW = receiver bandwidth, SSFP = steady state free precession, 3D = three-dimensional, VPS = views per segment.

discomfort and morbidity associated with transesophageal echocardiography or cardiac catheterization. It involves no ionizing radiation, which represents a distinct advantage over catheterization and CT, especially in pediatric patients who may need multiple examinations. No nephrotoxic contrast agents are used, and the prevalence of allergic and anaphylactoid reactions to gadolinium is significantly lower than that associated with the iodinated contrast material used for catheterization and CT (17).

Cardiac MR imaging provides excellent anatomic detail with a large field of view, vessel-specific flow data, and a method for assessing myocardial function. Although 2D Doppler echocardiography has dramatically improved the noninvasive evaluation of congenital heart disease, quantitative data about ventricular size (especially the RV) and valvular regurgitation are limited. Cardiac MR imaging can help quantify size, function, and the percentage of regurgitation. This information is particularly useful in older postsurgical patients, who often have poor acoustic windows that severely limit the diagnostic quality of ultrasonography. In addition, as experience increases and technical advances are made, cardiac MR imaging has the potential to be less operator dependent than echocardiography.

MR imaging is contraindicated when pacemakers or pacemaker wires are present, although this absolute contraindication is being critically reevaluated (18,19). Some types of implanted metallic stents and coils can limit image quality due to susceptibility artifacts. Arrhythmia or poor electrocardiographic signal rarely prevents adequate gating. Although cardiac MR imaging requires patient cooperation, including the ability to remain still and hold the breath, techniques can be modified for less cooperative and younger patients, so that not all pediatric studies need to be performed with the patient under general anesthesia. The disadvantages of cardiac MR imaging (relative to CT angiography) are longer scanning times and the need for greater operator expertise.

Basic Imaging Techniques

Technical information is summarized in Table 1.

Bright (white) blood imaging is the most frequently used sequence and generally provides the most diagnostic data.

Teaching Point

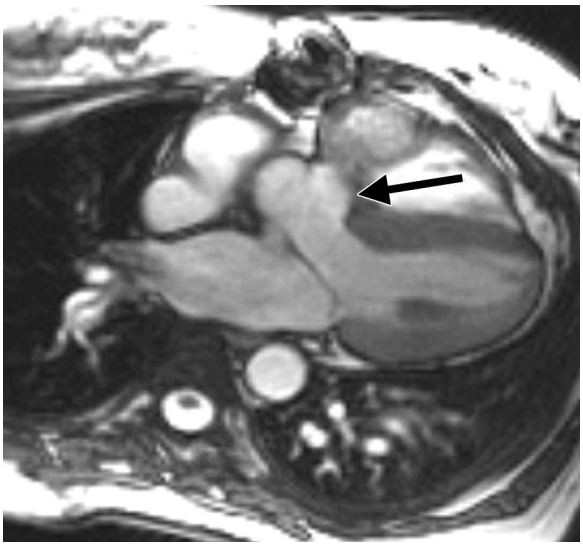

Figure 5. Axial SSFP image obtained in a 14-year-old girl with repaired TOF reveals an overriding aortic valve and a VSD patch (arrow).

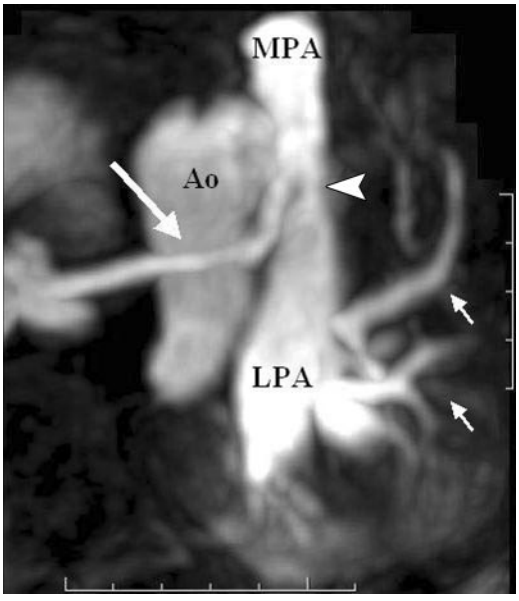

Figure 6. Axial oblique MIP image of the branch pulmonary arteries obtained in a 9-year-old boy with repaired TOF demonstrates severe long-segment narrowing of the right pulmonary artery (long arrow) and moderate narrowing (arrowhead) of the left pulmonary artery *(LPA)*. Short arrows indicate branches of the pulmonary veins. *Ao* = aorta, *MPA* = main pulmonary artery.

Electrocardiographically-gated SSFP imaging provides excellent contrast between the blood pool and the myocardium, with excellent in-plane spatial resolution and good temporal resolution (Fig 5). Although it is preferable to perform these sequences with breath holding (to eliminate diaphragmatic motion artifact), the technique can be modified for non-breath-hold imaging in less cooperative patients. Two-dimensional cinematographic (cine) MR images are obtained during one complete cardiac cycle, providing excellent anatomic detail and thereby allowing quantification of ventricular volumes and function. Modifications in smaller patients include reducing the field of view, the section thickness, and the number of views per segment to improve spatial and temporal resolution; and increasing the number of acquisitions to both maintain an adequate signal-to-noise ratio and average out diaphragm motion in free-breathing patients. With these adjustments, care must be taken to keep repetition time and echo time short, since artifacts related to the loss of steady state increase as repetition time and echo time increase. As with all MR imaging sequences, these trade-offs are greatly influenced by gradient speed and require flexibility on the part of the imager.

High-resolution gadolinium-enhanced 3D MR angiography is particularly valuable for imaging the branch pulmonary arteries, the aorta, and the systemic and pulmonary venous anatomy (Fig 6). The 3D data set can be reviewed at dedicated 3D workstations to improve diagnostic accuracy. This modality has proved accurate in the evaluation of branch pulmonary artery stenosis (4,16, 20) and of the systemic and pulmonary venous anatomy (1,21,22). Recently developed 3D imaging technology makes use of multiple surface coils for spatial localization, reducing the number of phase-encoded steps needed, which dramatically increases imaging speed while maintaining adequate spatial resolution. This time-resolved imaging is increasingly being used in pediatric and adult vascular applications (23,24) and, in pediatric patients, has great potential to allow time-resolved MR angiography during short breath holds

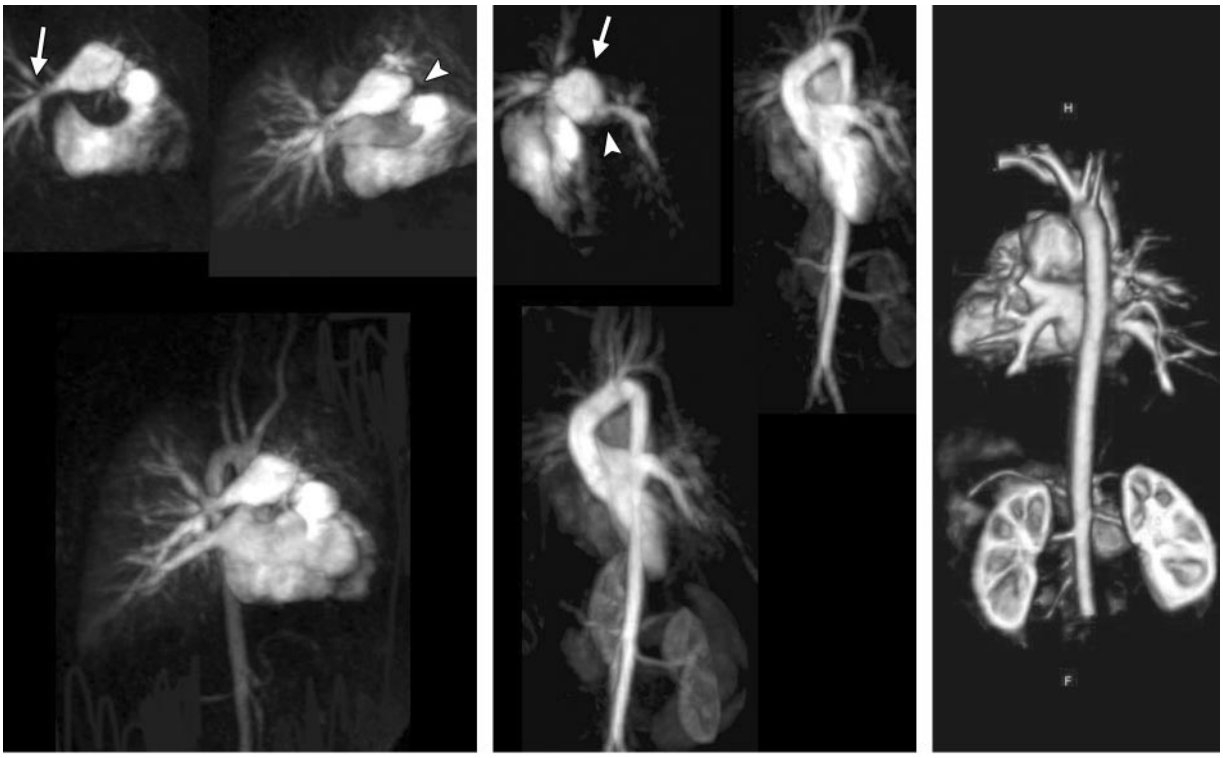

a. b. c.

Figure 7. Time-resolved imaging in a 7-year-old girl with repaired TOF. A set of 30 measurements was obtained at less than 1 second per volume, with a voxel size of 2.5 × 2.0 × 2.5 mm. **(a)** Coronal oblique MIP images. At the first dynamic (top left), peripheral stenosis (arrow) is seen in the right pulmonary artery. At the second dynamic (top right), severe obstruction at the level of a bioprosthetic pulmonary valve (arrowhead) is more clearly delineated. Note the perfusion of the right lung and the filling of the right pulmonary veins. The third dynamic (bottom) better demonstrates the aortic arch and right pulmonary veins. **(b)** Sagittal oblique MIP images obtained to evaluate the left pulmonary artery show peripheral stenosis (arrowhead) and aneurysmal dilatation (arrow) of the MPA. The third dynamic (bottom) demonstrates the left pulmonary veins, the aortic arch, and the thoracic and abdominal aorta. **(c)** Volume-rendered image (posterior view) from the same time-resolved data set (only one dynamic reconstructed) clearly depicts the pulmonary venous connections and aortic arch.

or free breathing, without sacrificing spatial resolution (Fig 7; see also Movie 1 at *radiographics.rsnajnls.org/cgi/content/full/26/1/197/DC1*).

Phase-contrast imaging makes use of an additional biphasic gradient to label moving voxels with a phase shift proportional to velocity within each voxel. With use of segmented k-space acquisition, cine images obtained during multiple cardiac cycles are displayed as both a magnitude image and a phase image (voxel intensity being dependent on phase shift) with good spatial and temporal resolution. The true temporal resolution is twice the repetition time multiplied by the number of views per segment. Care must be taken in pediatric imaging to adjust the number of views

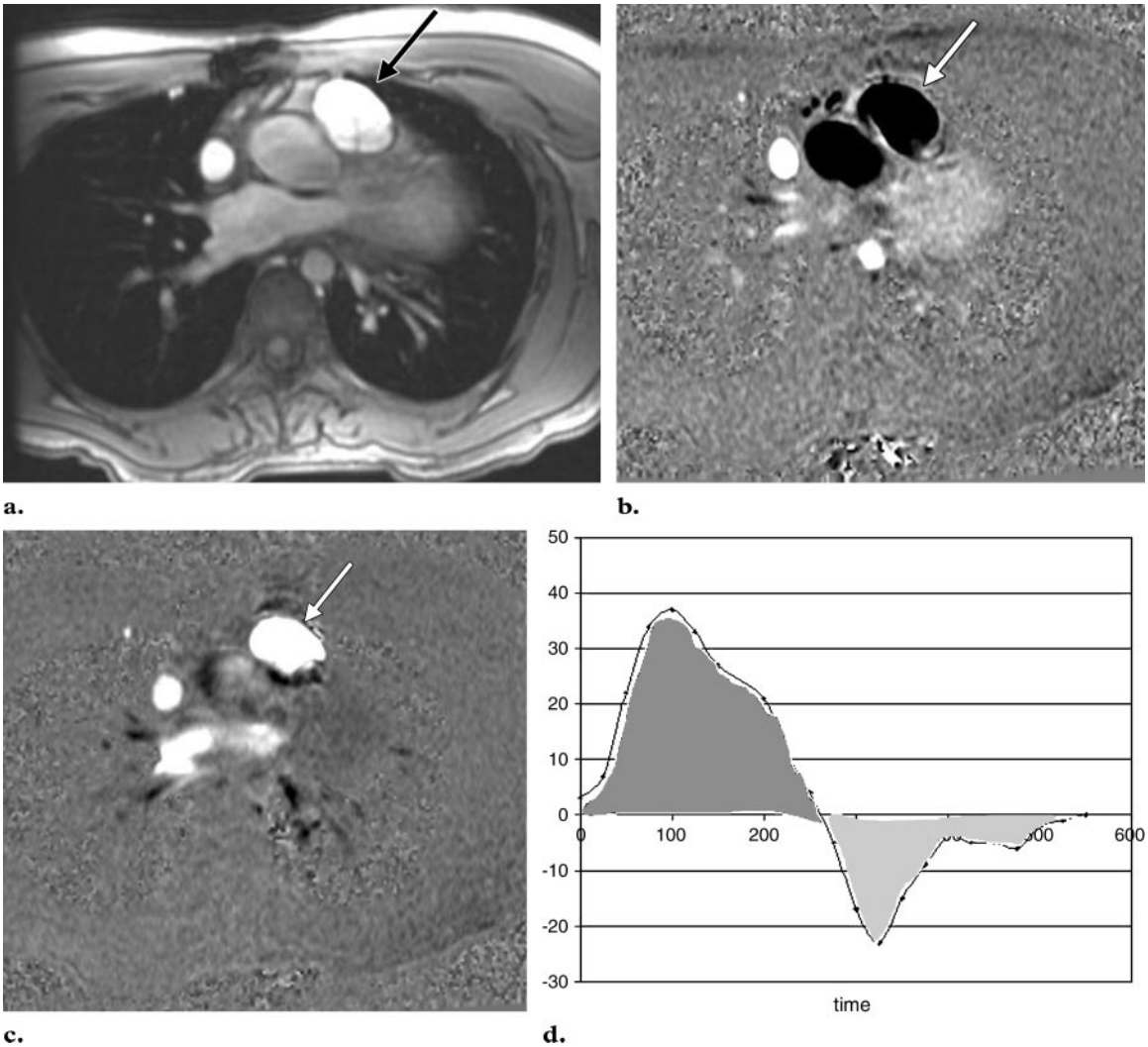

Figure 8. Phase-contrast imaging in a 14-year-old girl with repaired TOF and PR. **(a)** Magnitude image from a phase-contrast sequence shows the pulmonary artery (arrow) in cross section. **(b)** On a phase-velocity image obtained during systole, the signal intensity of the pulmonary artery (arrow) is proportional to through-plane velocity. **(c)** Phase-velocity image obtained during diastole reveals retrograde PR flow (arrow). **(d)** Graph illustrates flow (in milliliters per second) versus time (in milliseconds) during phase-contrast imaging. PR is the ratio of retrograde flow volume (regurgitation) (dark gray) to antegrade flow volume (light gray). Both volumes are measured in milliliters.

per segment, the voxel size, and the number of acquisitions to permit adequate temporal resolution and signal in smaller patients with faster heart rates. This technique allows accurate quantification of vessel flow, including shunt volumes and regurgitation volumes (Fig 8), and has been extensively validated both in vitro and in vivo (25–37).

Teaching Point

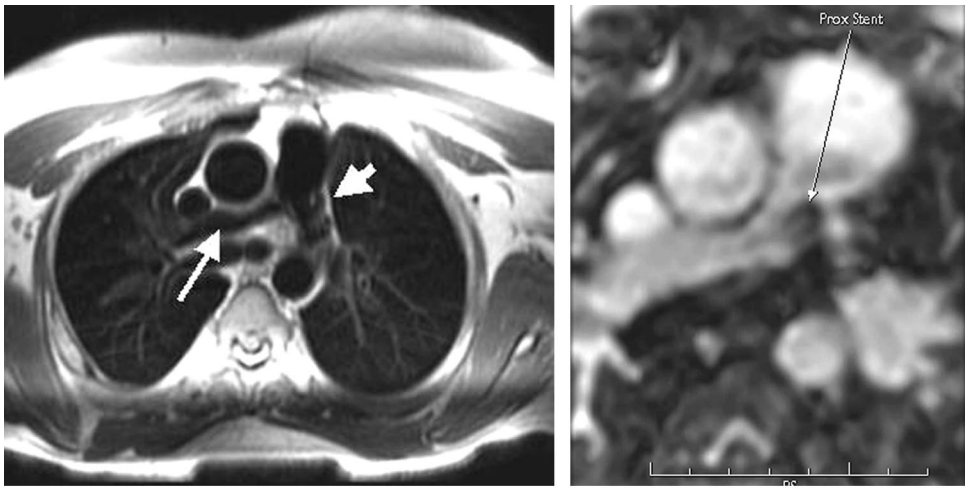

a. b.

Figure 9. FSE-DIR imaging versus SSFP imaging in an 18-year-old man with repaired TOF. **(a)** Axial FSE-DIR image obtained at the level of the branch pulmonary arteries reveals stenosis of the mid–right pulmonary artery (long arrow). Artifact from a stent in the left pulmonary artery is also seen (short arrow) but is less prominent than with gradient echo–based sequences. **(b)** MIP image reveals signal intensity loss in the left pulmonary artery secondary to the metallic stent. *Prox* = proximal.

Teaching Point

Black blood imaging makes use of an electrocardiographically-gated FSE-DIR sequence to provide 2D images of the heart and vasculature at end diastole. It provides excellent spatial resolution and is essential when imaging the airway, vessel wall anatomy, and pericardium. FSE-DIR imaging is particularly useful in defining the extent and location of branch pulmonary artery stenosis when turbulence or metal-related artifacts are present (Fig 9). RV–pulmonary artery conduits and proximal branch pulmonary arteries can often be clearly imaged in free-breathing younger patients by increasing the number of acquisitions to average out respiratory motion. This gain in signal can then be "traded in" for better in-plane resolution by increasing the matrix size. The cost of this approach is imaging time, which at times necessitates a more focused evaluation. Knowledge of the clinically relevant data becomes critical, especially when imaging less cooperative patients.

Assessment of Ventricular Mass, Volume, and Flow

In the assessment of patients who have undergone TOF repair, serial follow-up MR imaging examinations can be performed to measure RV size (volume and mass) and function, as well as to quantify the magnitude of PR or tricuspid regurgitation (TR). Contiguous standard short-axis images are obtained, and, with use of commercially available cardiac postprocessing software, the endocardium-blood border is traced to calculate end-diastolic volume and end-systolic volume (Fig 10).

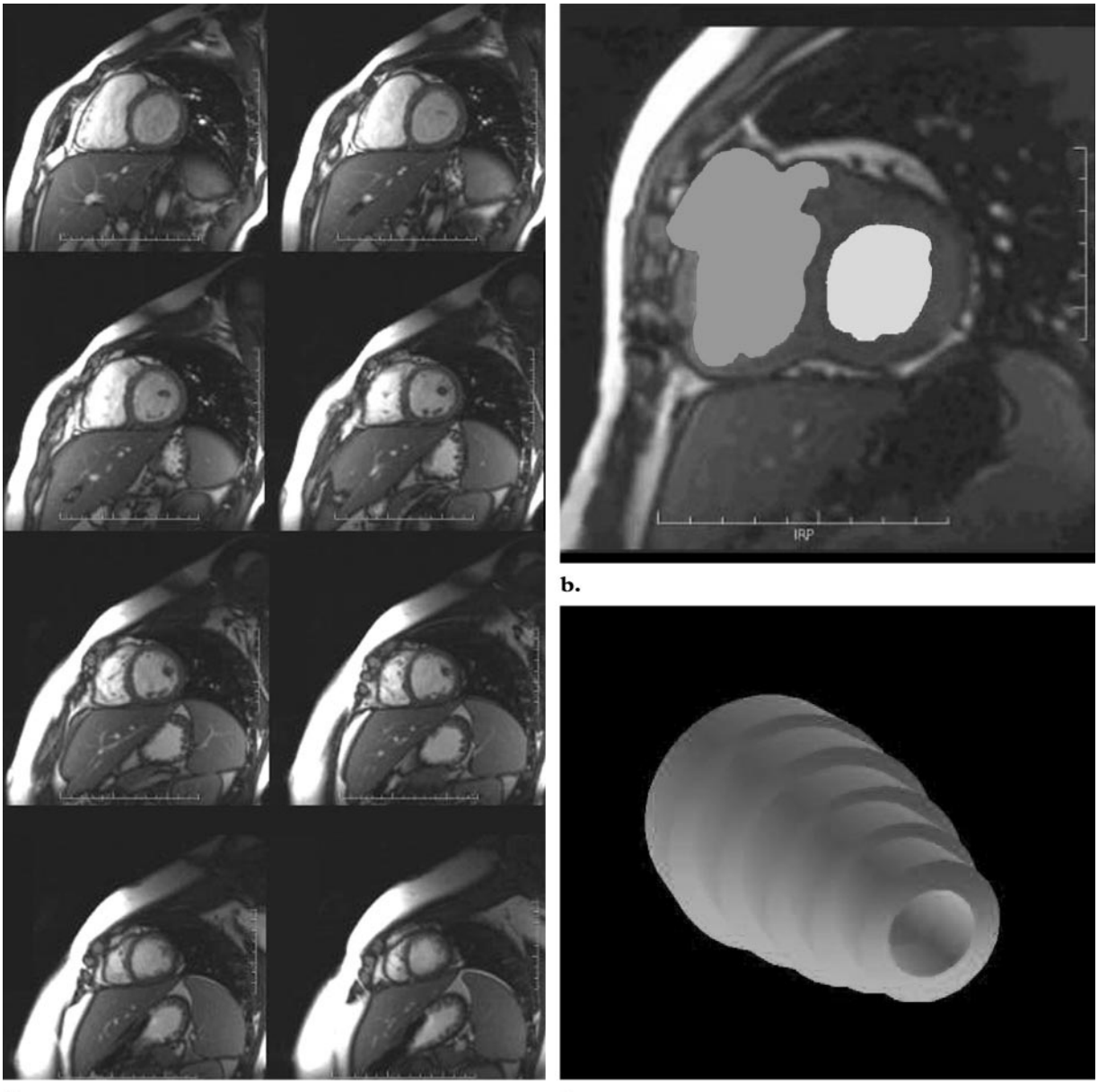

Figure 10. Calculation of end-diastolic volume and end-systolic volume. **(a)** Multiple contiguous short-axis SSFP images show the endocardial borders of the ventricular cavities. **(b)** Magnified view of a short-axis SSFP image shows the calculated end-diastolic areas of the right (dark gray) and left (light gray) ventricles. Because the section thickness is known, the end-diastolic volume for each section can be calculated. The total end-diastolic volume can then be obtained by summing the volumes for contiguous sections. **(c)** Drawing illustrates the ventricular volume for an idealized right ventricle.

Table 2
Normative Data for Cardiac MR Imaging

Parameter	Patients		
	Men	Women	Children*
Left ventricle			
End-diastolic volume (mL/m^2)	53–112	56–99	49–85
Ejection fraction (%)	55–73	54–74	>55
Mass (g/m^2)	46–83	37–67	55–107
Right ventricle			
End-diastolic volume (mL/m^2)	58–114	48–103	48–92
Ejection fraction (%)	48–63	50–70	>45
Mass (g/m^2)	16–36*	16–36*	20–32

Sources.—References 38 and 39.
*Data based on a segmented k-space fast gradient-echo sequence, not an SSFP sequence.

Once the volumes are calculated, the stroke volume, cardiac output, and ejection fraction can be calculated as follows: end-diastolic volume − end-systolic volume = stroke volume, stroke volume × heart rate = cardiac output, and stroke volume ÷ end-diastolic volume = ejection fraction.

The available normative data for men, women, and children (adjusted for body surface area) are provided in Table 2 (38,39). There is a clear lack of adequate normative data for children who are imaged with the newer SSFP sequence. This sequence provides a better signal-to-noise ratio—and hence, improved contrast between blood and myocardium—and has been shown to yield systematically different values for ventricular volumes than do the older gradient echo–based cine sequences (39). The lack of reliable normative MR imaging data for this subset of patients continues to be a problem and should be addressed with an appropriately designed investigation.

Quantification of regurgitation entails a postprocessing technique in which through-plane velocity and area are measured by tracing the vessel border on sequential phase-contrast images obtained over one cardiac cycle (Fig 8).

The phase-contrast imaging technique provides quantitative lung perfusion data and allows calculation of the ratio between pulmonary and systemic flow. These two applications have good agreement with nuclear lung perfusion (25,26) and catheter-derived pulmonary-systemic flow ratio (31,33), respectively. In contrast to hemodynamic assessment with catheterization, the phase-contrast imaging technique can be used to measure flow across any vessel, thereby allowing estimation of lung perfusion in patients with multiple sources of pulmonary blood flow.

Common Postoperative Complications

The goal of repair is to close the VSD and relieve RV outflow tract obstruction. Two basic approaches to repair have evolved: *(a)* early total repair and *(b)* palliative shunt creation (eg, Blalock-Taussig operation) followed by definitive repair. Complete repair in early infancy has the benefit of requiring only one operation and helps obviate palliative shunt creation, which adds a volume load to the LV until complete repair is performed.

If the pulmonary valve annulus is hypoplastic, a transannular patch is necessary. If the annulus is adequate, the repair can be limited to opening the RV outflow tract without crossing the annulus. VSD closure and infundibular muscle resection can be accomplished through an atrial incision, although a small ventriculotomy is often necessary for patch enlargement of the outflow area.

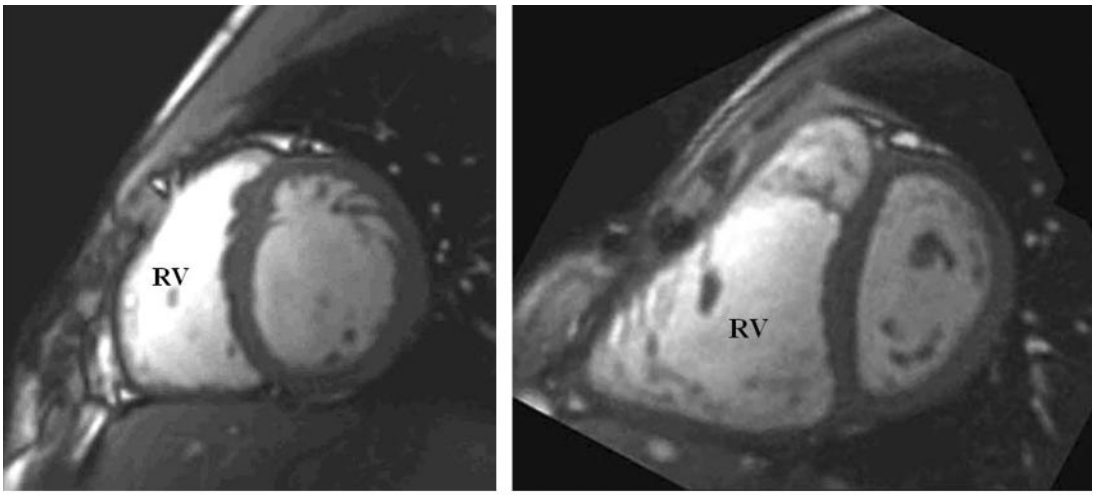

a. b.

Figure 11. Measurement of RV size and function with cardiac MR imaging. **(a)** SSFP image shows a normal RV. **(b)** SSFP image obtained in a 14-year-old boy with repaired TOF shows a dilated RV.

Residual VSD

Residual VSD, although rare, should be sought and excluded. Although most residual VSDs can be accurately diagnosed with 2D Doppler echocardiography, they can also be identified with SSFP imaging, and the magnitude of the shunt can be quantified with phase-contrast imaging. Prior to the advent of cardiac MR imaging, reliable shunt quantification was possible only with invasive catheterization. High-velocity shunting through a small VSD creates a "jet" of turbulent flow, which manifests as local loss of signal intensity or a signal void on SSFP images.

PR, RV Enlargement, and RV Dysfunction

Teaching Point

PR, the most common sequela of transannular or RV outflow tract patch repair, is present in nearly all TOF patients and can be accurately quantified with phase-contrast imaging. In addition, the effects of PR on RV size and function can be serially measured. Chronic PR is generally well tolerated; however, the evidence is beginning to point to PR as an important contributing cause of long-term morbidities, including atrial and ventricular arrhythmia, RV dilatation, and, possibly, sudden death (1,3,5,40–44). The combination of limited outcome data and suboptimal therapy (pulmonary valve replacement) leaves clinicians with no clear guidelines as to when chronic PR should be treated (10). Because cardiac MR imaging can accurately help quantify PR and RV ejection fraction, it will play a critical role in establishing better clinical management guidelines (see Movie 2 at *radiographics.rsnajnls.org/cgi/content/full/26/1/197/DC1*).

Cardiac MR imaging is the standard of reference for measuring RV size and function (Fig 11) (45,46). Although RV ejection fraction, like most ejection-phase indexes, is load dependent, it is presently the most accurate and reproducible criterion for assessing RV systolic function. Depressed RV ejection fraction is linked to adverse outcomes (47), and early detection, with intervention to preserve RV function, will likely contribute to better long-term outcome in TOF patients.

Residual Pulmonary Stenosis

Approximately 10%–15% of patients will have residual or recurrent branch pulmonary stenosis (5). A significant number of these patients will require additional surgery or catheter-directed angioplasty for residual or recurrent pulmonary stenosis. The level of stenosis varies from the proximal RV outflow tract to the distal branch

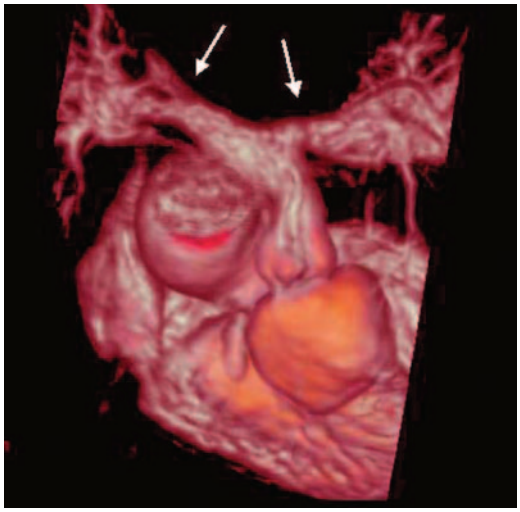

Figure 12. Pulmonary stenosis in a 12-year-old boy with repaired TOF. Volume-rendered image (superior view) shows a dilated infundibulum, some narrowing at the pulmonary valve level, and mild bilateral branch pulmonary stenosis (arrows).

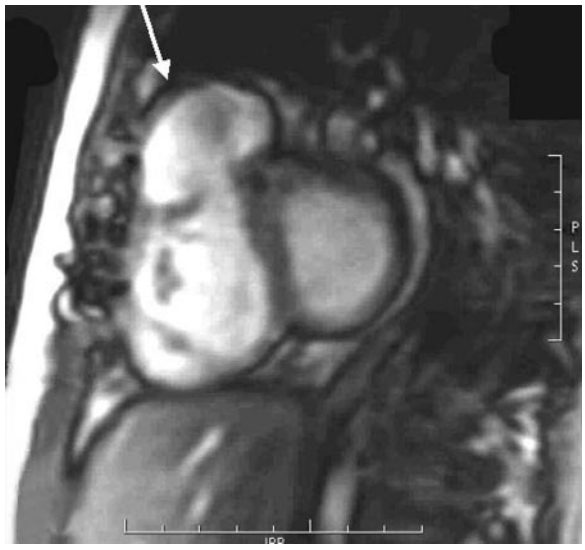

Figure 13. RV outflow tract aneurysm in a 10-year-old girl with repaired TOF. Short-axis SSFP image reveals aneurysmal dilatation of the RV outflow tract (arrow). Significant dyskinesia was noted at cine MR imaging.

pulmonary arteries, including surgically placed RV–pulmonary artery conduits (Fig 12).

Tricuspid Regurgitation

The prevalence of moderate or greater TR is estimated to be approximately 10% (5). TR is usually a consequence of progressive RV dilatation with subsequent annular dilatation of the tricuspid valve. The magnitude of the regurgitation can be quantified with phase-contrast imaging data either alone or in combination with RV volumetric data. Quantification of TR has yet to be vigorously validated, in part due to the lack of a robust standard of reference. Incorporating RV volumetric data with phase-contrast imaging data may have inherent error greater than that for semilunar (aortopulmonary) regurgitation. As with PR, the effects of TR on RV size can be assessed with RV volumetric data.

RV Outflow Tract Aneurysm

RV outflow tract aneurysms are often present and are related in part to transannular or RV outflow tract patching (Fig 13). Other possible contributing causes include extensive infundibular muscle resection and ischemic insult (48). The size of the RV outflow tract is easily and accurately evaluated with SSFP imaging, and reduced RV ejection fraction has been associated with the presence of RV outflow tract aneurysm (11) (see Movie 3 at *radiographics.rsnajnls.org/cgi/content/full/26/1/197/DC1*). The significance of this finding is unclear in that, by definition, dyskinesis results in a reduction of global ejection fraction; how this relates to contractile function at the myocardial level is less clear. In the measurement of the RV volumes, inclusion of the dyskinetic segment necessarily "contaminates" global ejection fraction, potentially exaggerating the degree of myocardial contractile dysfunction when the RV sinus actually has normal regional shortening (49). The inefficient transfer of stroke volume to the pulmonary arteries may play a part in the presence and progression of reduced cardiac output and exercise intolerance.

Conduit Obstruction

Because of the lack of durable long-term RV–pulmonary artery conduits, obstruction eventually develops in nearly all patients who require a conduit as a part of initial repair. Conduit obstruction can be identified with multiple imaging sequences. However, the ability to determine the degree of

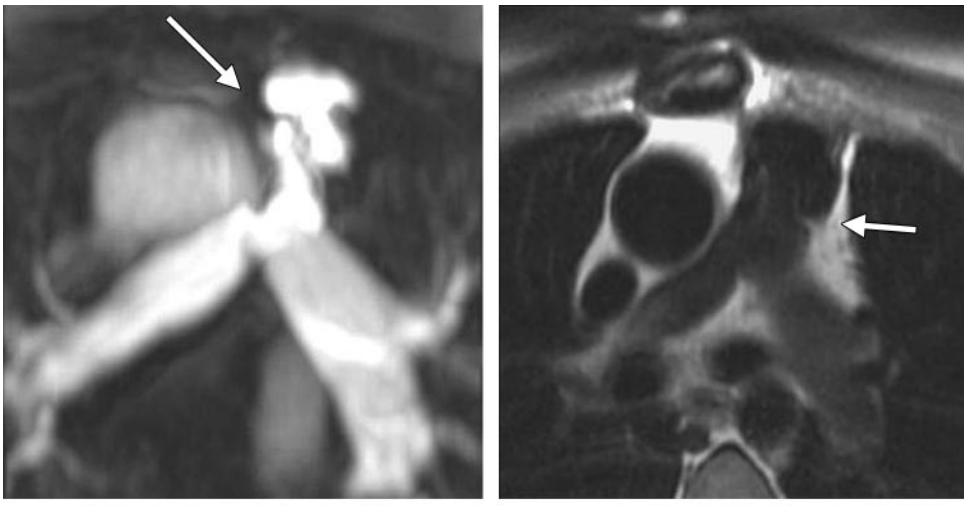

a. b.

Figure 14. Conduit obstruction in a 25-year-old man with repaired TOF. **(a)** MIP image of an RV–pulmonary artery conduit suggests narrowing at the anastomosis (arrow). However, the image is degraded by artifact from metallic material within the conduit. **(b)** On a 2D FSE-DIR image, the narrowing (arrow) is still evident but is not as severe as was suggested by findings at bright (white) blood imaging.

obstruction is somewhat limited compared with the accuracy of diagnosing branch pulmonary stenosis. Artifacts related to metal within the conduit and to turbulent flow often interfere with this assessment. As previously mentioned, 2D FSE-DIR imaging is less affected by these artifacts and can often provide diagnostic information (Fig 14). Fortunately, Doppler gradients can be obtained in almost all patients, even those with poor acoustic windows, and correlate well with catheter-derived gradients. This approach is a good example of recognizing and using the individual strengths of both echocardiography and cardiac MR imaging to obtain complementary diagnostic data.

LV Dysfunction

The accuracy and reliability of cardiac MR imaging in measuring LV systolic function is well established (50). In addition to its previously mentioned advantages over echocardiography, cardiac MR imaging–derived LV ejection fraction retains its accuracy in the presence of RV volume overload (diastolic septal flattening) and abnormal septal motion, unlike echocardiography-derived shortening fraction (50). LV dysfunction is an uncommon complication but has been associated with a number of predictors, including time elapsed since palliative arterial shunt creation, aortic regurgitation, and, most significantly, RV ejection fraction (47,48,51,52). Recently, LV ejection fraction was found to be the strongest predictor of poor clinical status (47). Proposed mechanisms include akinesia resulting from the VSD patch, septal fibrosis, chronic volume loading from early palliative shunt creation, abnormal septal motion, and myocardial injury at the time of repair.

Conclusions

With technologic advances over the past decade, cardiac MR imaging has evolved as the ideal clinical modality for evaluating patients who have undergone TOF repair. Further advances are likely to bring about new applications, better normative data, and more examinations that are operator independent. As this patient population continues to age, cardiac MR imaging will likely contribute significantly to their care. Reliable serial cardiac MR imaging data can help determine when to intervene to preserve ventricular function and improve long-term outcome.

References

1. Helbing WA, de Roos A. Clinical applications of cardiac magnetic resonance imaging after repair of tetralogy of Fallot. Pediatr Cardiol 2000;21:70–79.
2. Nadas AS. Tetralogy of Fallot. In: Fyler DC, ed. Nadas' pediatric cardiology. Philadelphia, Pa: Hanley & Belfus, 1992.
3. Nollert G, Fischlein T, Bouterwek S, Bohmer C, Klinner W, Reichart B. Long-term survival in patients with repair of tetralogy of Fallot: 36-year follow-up of 490 survivors of the first year after surgical repair. J Am Coll Cardiol 1997;30:1374–1383.
4. Murphy JG, Gersh BJ, Mair DD, et al. Long-term outcome in patients undergoing surgical repair of tetralogy of Fallot. N Engl J Med 1993;329:593–599.
5. Gatzoulis MA, Balaji S, Webber SA, et al. Risk factors for arrhythmia and sudden cardiac death late after repair of tetralogy of Fallot: a multicentre study. Lancet 2000;356:975–981.
6. Bacha EA, Scheule AM, Zurakowski D, et al. Long-term results after early primary repair of tetralogy of Fallot. J Thorac Cardiovasc Surg 2001;122:154–161.
7. Lillehei CW, Varco RL, Cohen M, et al. The first open heart corrections of tetralogy of Fallot: a 26–31 year follow-up of 106 patients. Ann Surg 1986;204:490–502.
8. Discigil B, Dearani JA, Puga FJ, et al. Late pulmonary valve replacement after repair of tetralogy of Fallot. J Thorac Cardiovasc Surg 2001;121:344–351.
9. Vliegen HW, van Straten A, de Roos A, et al. Magnetic resonance imaging to assess the hemodynamic effects of pulmonary valve replacement in adults late after repair of tetralogy of Fallot. Circulation 2002;106:1703–1707.
10. Therrien J, Siu SC, McLaughlin PR, Liu PP, Williams WG, Webb GD. Pulmonary valve replacement in adults late after repair of tetralogy of Fallot: are we operating too late? J Am Coll Cardiol 2000;36:1670–1675.
11. van Straten A, Vliegen HW, Hazenkamp MG, et al. Right ventricular function after pulmonary valve replacement in patients with tetralogy of Fallot. Radiology 2004;233:824–829.
12. Yemets IM, Williams WG, Webb GD, et al. Pulmonary valve replacement late after repair of tetralogy of Fallot. Ann Thorac Surg 1997;64:526–530.
13. Lim C, Lee JY, Kim WH, et al. Early replacement of pulmonary valve after repair of tetralogy: is it really beneficial? Eur J Cardiothorac Surg 2004;25:728–734.
14. Warner KG, Anderson JE, Fulton DR. Restoration of the pulmonary valve reduces right ventricular volume overload after previous repair of tetralogy of Fallot. Circulation 1993;88(5 pt 2):II189–II197.
15. Eyskens B, Reybrouck T, Boagaert J, et al. Homograft insertion for pulmonary regurgitation after repair of tetralogy of Fallot improves cardiorespiratory exercise performance. Am J Cardiol 2000;85:221–225.
16. Geva T, Greil GR, Marshall AC, Landzberg M, Powell AJ. Gadolinium-enhanced 3-dimensional magnetic resonance angiography of pulmonary blood supply in patients with complex pulmonary stenosis or atresia: comparison with x-ray angiography. Circulation 2002;106:473–478.
17. Cochran ST, Bomyea K, Sayre JW. Trends in adverse events after IV administration of contrast media. AJR Am J Roentgenol 2001;176(6):1385–1388.
18. Loewy J, Loewy A, Kendall EJ. Reconsideration of pacemakers and MR imaging. RadioGraphics 2004;24(5):1257–1268.
19. Martin ET, Coman JA, Shellock FG, Pulling CC, Fair R, Jenkins K. Magnetic resonance imaging and cardiac pacemaker safety at 1.5 Tesla. J Am Coll Cardiol 2004;43(7):1315–1324.
20. Kondo C, Takada K, Yokoyama U, et al. Comparison of three-dimensional contrast-enhanced magnetic resonance angiography and axial radiographic angiography for diagnosing congenital stenoses in small pulmonary arteries. Am J Cardiol 2001;87:420–424.
21. Greil GF, Powell AJ, Gildein HP, Geva T. Gadolinium-enhanced three-dimensional magnetic resonance angiography of pulmonary and systemic venous anomalies. J Am Coll Cardiol 2002;39:335–341.
22. Neimatallah MA, Ho VB, Dong Q, et al. Gadolinium-enhanced 3D magnetic resonance angiography of the thoracic vessels. J Magn Reson Imaging 1999;10:758–770.
23. van den Brink JS, Watanabe Y, Kuhl C, et al. Implications of SENSE MR in routine clinical practice. Eur J Radiol 2003;46:3–27.
24. Chung T, Muthupillai R. Application of SENSE in clinical pediatric body MR imaging. Top Magn Reson Imaging 2004;15(3):187–196.
25. Silverman JM, Julien PJ, Herfkens RJ, Pele NJ. Quantitative differential pulmonary perfusion: MR imaging versus radionuclide lung scanning. Radiology 1993;189:699–701.
26. Fratz S, Hess J, Schwaiger M, Martinoff S, Stern HC. More accurate quantification of pulmonary blood flow by magnetic resonance imaging than by lung perfusion scintigraphy in patients with fontan circulation. Circulation 2002;106(12):1510–1513.
27. Maier SE, Meier D, Boesiger P, et al. Human abdominal aorta: comparative measurements of blood flow with MR imaging and multigated Doppler US. Radiology 1989;171:487–492.
28. Meier D, Maier S, Boesiger P. Quantitative flow measurements on phantoms and on blood vessels with MR. Magn Reson Med 1988;8:25–34.

29. Kondo C, Caputo GR, Semelka R, et al. Right and left ventricular stroke volume measurements with velocity-encoded cine MR imaging: in vitro and in vivo validation. AJR Am J Roentgenol 1991;157:9–16.
30. Sieverding L, Jung WI, Klose U, et al. Noninvasive blood flow measurement and quantification of shunt volume by cine magnetic resonance in congenital heart disease: preliminary results. Pediatr Radiol 1992;22:48–54.
31. Powell AJ, Maier SE, Chung T, Geva T. Phase-velocity cine magnetic resonance imaging measurement of pulsatile blood flow in children and young adults: in vitro and in vivo validation. Pediatr Cardiol 2000;21:104–110.
32. Firmin DN, Nayler GL, Klipstein RH, Underwood SR, Rees RS, Longmore DB. In vivo validation of MR velocity imaging. J Comput Assist Tomogr 1987;11:751–756.
33. Beerbaum P, Korperich H, Barth P, Esdorn H, Gieseke J, Meyer H. Noninvasive quantification of left-to-right shunt in pediatric patients: phase-contrast cine magnetic resonance imaging compared with invasive oximetry. Circulation 2001;103(20): 2476–2482.
34. Powell AJ, Tsai-Goodman B, Prakash A, Greil GF, Geva T. Comparison between phase-velocity cine magnetic resonance imaging and invasive oximetry for quantification of atrial shunts. Am J Cardiol 2003;91(12):1523–1525, A9.
35. Brenner LD, Caputo GR, Mostbeck G, et al. Quantification of left to right atrial shunts with velocity-encoded cine nuclear magnetic resonance imaging. J Am Coll Cardiol 1992;20(5):1246–1250.
36. Arheden H, Holmqvist C, Thilen U, et al. Left-to-right cardiac shunts: comparison of measurements obtained with MR velocity mapping and with radionuclide angiography. Radiology 1999;211:453–458.
37. Greil G, Geva T, Maier SE, Powell AJ. Effect of acquisition parameters on the accuracy of velocity encoded cine magnetic resonance imaging blood flow measurements. J Magn Reson Imaging 2002; 15:47–54.
38. Lorenz CH. The range of normal values of cardiovascular structures in infants, children and adolescents by magnetic resonance imaging. Pediatr Cardiol 2000;21:37–46.
39. Alfakih K, Plein S, Thiele H, Jones T, Ridgway JP, Sivananthan MU. Normal human left and right ventricular dimensions for MRI as assessed by turbo gradient echo and steady-state free precession imaging sequences. J Magn Reson Imaging 2003;17:323–329.
40. Kugler JD. Predicting sudden death in patients who have undergone tetralogy of Fallot repair: is it really as simple as measuring ECG intervals? J Cardiovasc Electrophysiol 1998;9:103–106.
41. Marie PY, Marcon F, Brunotte F, et al. Right ventricular overload and induced sustained ventricular tachycardia in operatively "repaired" tetralogy of Fallot. Am J Cardiol 1992;69:785–789.
42. Silka MJ, Hardy BG, Menashe VD, Morris CD. A population-based prospective evaluation of risk of sudden cardiac death after operation for common congenital heart defects. J Am Coll Cardiol 1998; 32:245–251.
43. Gatzoulis MA, Till JA, Somerville J, Redington AN. Mechano-electrical interaction in tetralogy of Fallot: QRS prolongation relates to right ventricular size and predicts malignant ventricular arrhythmias and sudden death. Circulation 1995;92:231–237.
44. Bricker JT. Sudden death and tetralogy of Fallot: risks, markers, and causes. Circulation 1995;92: 158–159.
45. Shors SM, Fung CW, Finn PJ, Fieno DS. Accurate quantification of right ventricular mass at MR imaging by using cine true fast imaging with steady-state precession: study in dogs. Radiology 2004;230:383–388.
46. Grothues F, Moon JC, Bellenger NG, et al. Interstudy reproducibility of right ventricular volumes, function, and mass with cardiovascular magnetic resonance. Am Heart J 2004;147:218–223.
47. Geva T, Sandweiss BM, Gauvreau K, Lock JE, Powell AJ. Factors associated with impaired clinical status in long-term survivors of tetralogy of Fallot repair evaluated by magnetic resonance imaging. J Am Coll Cardiol 2004;43:1068–1074.
48. Davlouros PA, Kilner PJ, Hornung TS, et al. Right ventricular function in adults with repaired tetralogy of Fallot assessed with cardiovascular magnetic resonance imaging: detrimental role of right ventricular outflow aneurysms or akinesia and adverse right-to-left ventricular interaction. J Am Coll Cardiol 2002;40:2044–2052.
49. Lytrivi ID, Ko HH, Srivastava S, et al. Regional differences in right ventricular systolic function as determined by cine-magnetic resonance imaging following infundibulotomy. Am J Cardiol 2004; 94:970–973.
50. Bellenger NG, Burgess MI, Ray SG, et al. CHRISTMAS study steering committee and investigators: comparison of left ventricular ejection fraction and volumes in heart failure by echocardiography, radionuclide ventriculography and cardiovascular magnetic resonance—are they interchangeable? Eur Heart J 2000;21:1387–1396.
51. Kondo C, Nakazawa M, Kusakabe K, Momma K. Left ventricular dysfunction on exercise long-term after total repair of tetralogy of Fallot. Circulation 1995;92(9 suppl):II250–II255.
52. Niezen RA, Helbing WA, van Der Wall EE, van Der Geest RJ, Vliegen HW, de Roos A. Left ventricular function in adults with mild pulmonary insufficiency late after Fallot repair. Heart 1999; 82:697–703.

This article meets the criteria for 1.0 category 1 credit toward the AMA Physician's Recognition Award. To obtain credit, see www.rsna.org/education/rg_cme.html.

Teaching Points for Cardiac MR Imaging Assessment Following Tetralogy of Fallot Repair

Karen I. Norton, MD

RadioGraphics 2006; 26:197–211 • **Published online** 10.1148/rg.261055064 • **Content Codes:** CA MR PD

Page 198
After undergoing repair, patients commonly have a variable degree of pulmonary regurgitation (PR). Over long-term follow-up, right ventricular (RV) dilatation and dysfunction, atrial and ventricular arrhythmias, congestive heart failure, and sudden death may occur.

Page 200
Bright (white) blood imaging is the most frequently used sequence and generally provides the most diagnostic data.

Page 203
This technique allows accurate quantification of vessel flow, including shunt volumes and regurgitation volumes (Fig 8), and has been extensively validated both in vitro and in vivo (25–37).

Page 204
Black blood imaging makes use of an electrocardiographically-gated FSE-DIR sequence to provide 2D images of the heart and vasculature at end diastole. It provides excellent spatial resolution and is essential when imaging the airway, vessel wall anatomy, and pericardium. FSE-DIR imaging is particularly useful in defining the extent and location of branch pulmonary artery stenosis when turbulence or metal-related artifacts are present.

Page 207
PR, the most common sequela of transannular or RV outflow tract patch repair, is present in nearly all TOF patients and can be accurately quantified with phase-contrast imaging. In addition, the effects of PR on RV size and function can be serially measured. Chronic PR is generally well tolerated; however, the evidence is beginning to point to PR as an important contributing cause of long-term morbidities, including atrial and ventricular arrhythmia, RV dilatation, and, possibly, sudden death (1, 3, 5, 40–44).